The Influence of ENSO on Decadal Variations in the Relationship between the East Asian and Western North Pacific Summer Monsoons

SO-YOUNG YIM

School of Earth and Environmental Sciences, Seoul National University, Seoul, South Korea

SANG-WOOK YEH

Korea Ocean Research and Development Institute, Ansan, South Korea

RENGUANG WU

Center for Ocean–Land–Atmosphere Studies, Calverton, Maryland

JONG-GHAP JHUN

School of Earth and Environmental Sciences, Seoul National University, Seoul, South Korea

(Manuscript received 14 March 2007, in final form 1 October 2007)

ABSTRACT

A recent study suggested that the relationship between the East Asian summer monsoon (EASM) and the western North Pacific summer monsoon (WNPSM) experienced a decadal change around 1993–94. Based on a longer-term integration of a hybrid coupled model, the present study investigates decadal variations in the relationship between the EASM and the WNPSM. Apparent decadal variations in the above relationship have been identified in the model simulation.

The authors have analyzed the spatial pattern and variability during strong and weak EASM–WNPSM correlation periods. The purpose of this study is to understand potential reasons for decadal variations in the relationship between the two submonsoons. It is found that the precipitation variability associated with the WNPSM (ENSO) is enhanced over the East Asia and western North Pacific regions during periods when the EASM–WNPSM relationship is strong (weak). The large variability in precipitation associated with the WNPSM during strong periods strengthens the Pacific–Japan-like atmospheric teleconnection from the tropical western Pacific. In contrast, the Pacific–Japan-like pattern is not significant during weak periods. On the other hand, the large ENSO amplitude during weak periods results in an enhanced precipitation variability associated with ENSO. The results suggest that ENSO can destructively interfere with the relationship between the EASM and the WNPSM.

1. Introduction

The Asian–Pacific summer monsoon can be divided into three subsystems, that is, the East Asian summer monsoon (EASM), the western North Pacific summer monsoon (WNPSM), and the Indian summer monsoon (Wang and LinHo 2002). Figure 1 shows the spatial location of the three subsystems. The Indian summer monsoon and WNPSM are tropical monsoons, and the EASM is considered a subtropical monsoon. Earlier studies have investigated structures and main components of each monsoon subsystem (Krishnamurti 1985; Tao and Chen 1987; Chen et al. 1992; Murakami and Matsumoto 1994). Many recent studies emphasize the connections among them (Wang and Fan 1999; Wang et al. 2003). [Previous studies investigated the influence of WNPSM on EASM (Lau et al. 2000; Wang et al. 2001; Wu and Wang 2002; Wu et al. 2003); the influence of the Indian summer monsoon on EASM (Kripalani and Kulkarni 2001; Krishnan and Sugi 2001; Wu and Wang 2002); and the connections between the Indian summer monsoon and WNPSM (Wang and Xu 1997; Terray et al. 2003).]

Corresponding author address: Sang-Wook Yeh, Korea Ocean Research and Development Institute, 1270 Sa-2-dong, Ansan, 426-744, South Korea.
E-mail: swyeh@kordi.re.kr

DOI: 10.1175/2007JCLI1948.1

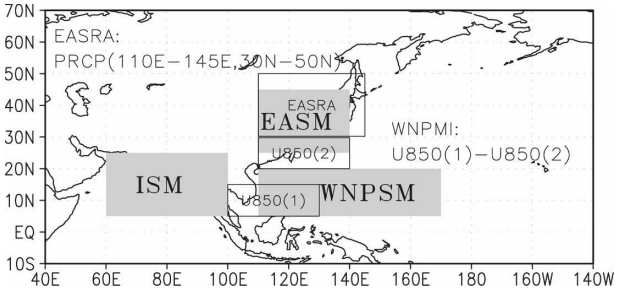

FIG. 1. The spatial location of the three subsystems, i.e., the Indian summer monsoon (ISM), the western North Pacific summer monsoon (WNPSM), and the East Asian summer monsoon (EASM), and schematic regions to calculate the monsoon indices.

The EASM covers eastern China, Japan, and Korea and it is associated with the rainfall variability along the so-called Mei-yu, Baiu, and Changma frontal bands, respectively. These major rainbands stretch over thousands of kilometers and affect the regional climate. The EASM is controlled by both tropical and subtropical influences (Tao and Chen 1987; Lee et al. 2005). The relationship between the EASM and tropical sea surface temperature (SST) has been the long-standing subject of many studies in the past decade (Huang and Wu 1989; Liu and Ding 1992; Shen and Lau 1995; Zhang et al. 1996; Chang et al. 2000; Wang et al. 2000; Lau and Weng 2001; Wu et al. 2003). It was found that there is a strong biennial signal in the correlations between the EASM and the tropical Pacific SST (Shen and Lau 1995). Yoo et al. (2004) showed that very different atmospheric circulation patterns appeared over East Asia during the summers of 1993 and 1994, which are associated with the SST variability in the western North Pacific (WNP) region. Furthermore, Chang et al. (2000) argued that there are interdecadal variations in the relationship between the EASM and the tropical Pacific SST and attributed these to interdecadal changes in the basic state of SST and winds in the Pacific. Wu and Wang (2002) also showed that there are changes in the interannual relationship between the EASM and El Niño–Southern Oscillation (ENSO) in the late 1970s, which is concurrent with the so-called Pacific climate shift (Graham 1994).

Recently, the relationship between the EASM and the WNPSM has received much attention. The WNPSM is an oceanic monsoon system and is mainly driven by the meridional gradient of SST (Tao and Chen 1987). The WNPSM circulation is characterized by a northwest–southeast oriented monsoon trough with intense precipitation, low-level southwesterlies, and upper-tropospheric easterlies (Murakami and Matsumoto 1994). A strong linkage in the meridional direction among the climatic factors in East Asia and the WNP (Wang et al. 2001; Lu 2004) has been noted. For instance, the convective activity over the WNP displays pronounced interannual variability and has considerable impacts on weather and climate over East Asia (Nitta 1987; Wu and Wang 2000; Wang et al. 2001; Lu 2004; Lee et al. 2005; Lee et al. 2006). The summer-mean precipitation anomaly over the East Asia region exhibits a tendency to be negatively correlated with the intensity of the WNPSM (Lau et al. 2000). Lee et al. (2005, 2006) argued that the intensity of the anomalous WNP subtropical high is a key factor in the EASM variation. Furthermore, Kwon et al. (2005, hereafter K05) recently argued that the relationship between the EASM and the WNPSM is much stronger in the recent decade (1994–2004) than in the epoch before 1994 (1979–93). This suggests that the EASM–WNPSM relationship has experienced a significant decadal change around 1993–94. K05 showed that the leading mode of summer-mean precipitation over the East Asia and WNP region has changed from a so-called ENSO-related mode in the period from 1979 to 1993 to a WNPSM-related mode in the recent decade (1994–2004).

The results in K05 raise questions regarding the decadal variation of the EASM–WNPSM relationship. Because of the short target period (1979–2004), K05 was able to analyze only a decadal change in the EASM–WNPSM relationship. The current study aims to identify decadal variations in the relationship between the EASM and the WNPSM in a long-term simulation using a hybrid coupled model (HCM). We also suggest a possible mechanism responsible for such low-frequency variations. Section 2 describes the model and methodology. In section 3, we briefly describe the performance of the HCM used in this study. We show the rainfall variability and decadal variations in the relationship between the EASM and the WNPSM simulated in the HCM and its possible mechanism in section 4. Our summary is given in section 5.

2. Model and methodology

a. Model

The HCM presented here was developed by Yeh (2001). The HCM applies a coupling strategy similar to that originally developed by Kirtman and Zebiak (1997). The HCM has a complex atmospheric general circulation model (AGCM) coupled to the ocean component of the Zebiak and Cane (ZC) ocean model (Zebiak and Cane 1987) in the tropical Pacific region (19°N–19°S, 130°E–90°W,). Outside the oceanic model domain, SSTs for the AGCM are prescribed based on the observed annually varying climatology. The atmo-

spheric component is the Seoul National University AGCM (SNUAGCM) (Kim et al. 1998), which is a global spectral model with T31 resolution (approximately 2.5° latitude × 3.5° longitude). There are 17 unevenly spaced sigma-coordinate vertical levels in the model. The SNUAGCM is based on the Center for Climate System Research/National Institute of Environmental Studies (CCSR/NIES) AGCM of Tokyo University (Numaguti et al. 1995) but has some major changes including the land surface process, shallow convection, and PBL processes (Kim et al. 1998). The ocean component is the ZC ocean model described by linear shallow-water equations, which produce thermocline depth anomalies and depth-averaged baroclinic currents. The annual cycles of the prescribed mean currents, temperature, and thermocline depth are included in the model. The ZC ocean model used in this study has a new parameterization for the temperature of subsurface water entrained into the ocean mixed layer (Yeh 2001).

In coupling the SNUAGCM to the ZC ocean model, we use an anomaly coupling strategy, following Kirtman and Zebiak (1997). Given a SST field, the AGCM produces a total wind stress field that has been empirically corrected (Huang and Shukla 1997). The AGCM wind stress climatology is subtracted and the wind stress anomalies are passed to the ocean component. The AGCM wind stress climatology is computed with respect to an uncoupled simulation with observed SST for the period from 1979 to 1996. Given a wind stress anomaly, the ZC ocean model produces a predicted SST anomaly (SSTA) in the tropical Pacific. The SSTA is superimposed on the observed annually varying global SST climatology and is then passed to the AGCM. The coupling frequency of the model is once every 10 days with mean values being exchanged between the ocean and the atmosphere. The advantage of the anomaly coupling strategy is to prevent the rapid climate drift seen in coupled models. The HCM is integrated for 159 years for this study. This is an additional integration from the HCM simulation analyzed by Yeh et al. (2004).

b. Methodology

In the present study, the EASM variability is measured using the summer-mean [June–August (JJA)] rainfall anomaly averaged over the East Asia region (30°–50°N, 115°–150°E), following Lee et al. (2005). For convenience, this East Asian summer rainfall anomaly is used as an index that represents the EASM variability. The WNPSM variability is measured by using two indices. The first one is a dynamical monsoon index defined by Wang et al. (2001). This WNP monsoon index (WNPMI) is defined as the difference of 850-hPa zonal wind anomalies between two areas (5°–15°N, 100°–130°E) and (20°–30°N, 110°–140°E). The other one is a rainfall index, defined by the summer-mean rainfall anomaly averaged over the WNP region (10°–20°N, 120°–150°E). For simplicity, this index is referred to as the WNP rainfall anomaly. Figure 1 shows the regions used to calculate these indices. K05 showed that the WNP rainfall anomaly and WNPMI are highly correlated (0.81) during the period from 1979 to 2004. As in observations, the simulated WNP rainfall anomaly and WNPMI are also well correlated with the simultaneous correlation coefficient, 0.90 for the entire period. In this study we use both WNPMI and WNP rainfall anomaly to measure variability of the WNPSM. In addition, the present study uses the Niño-3 SST index, defined as the averaged SST anomalies (SSTAs) over the Niño-3 region (5°N–5°S, 90°–150°W), as an ENSO index. Note that all indices used in this study are the same as those in K05.

Some model results presented herein are compared with the corresponding observation fields obtained from the Climate Prediction Center (CPC) Merged Analysis of Precipitation (CMAP) dataset for the period from 1979 to 2004 (Xie and Arkin 1997), the reanalysis products of the National Centers for Environmental Prediction (NCEP) (Kalnay et al. 1996), and monthly mean observed SST data for the period of 1950–2006, which were recently released by the National Climatic Data Center (Smith and Reynolds 2004).

3. Model performance

The performance of SNUAGCM has been rigorously tested by Kang et al. (2002) in terms of the climatological variations of summer monsoon rainfall in the Climate Variability and Predictability (CLIVAR)/Monsoon Intercomparison Project. According to Kang et al. (2002), the SNUAGCM simulates excessive precipitation in the subtropical western Pacific, but the maximum precipitation is shifted to the north by 5°–10° compared to observations. The model composite of SNUAGCM produced a stronger than observed monsoon circulation around the Asian continent; in particular the strong monsoon westerlies penetrate all the way to the western Pacific, resulting in heavy precipitation in the subtropical western Pacific. Yeh (2001) tested the performance of the HCM in terms of the 500-hPa geopotential height in comparisons with observations and showed that the dominant mode of 500-hPa geopotential height variability exhibits a notable spatial correspondence with the Pacific–North America pattern,

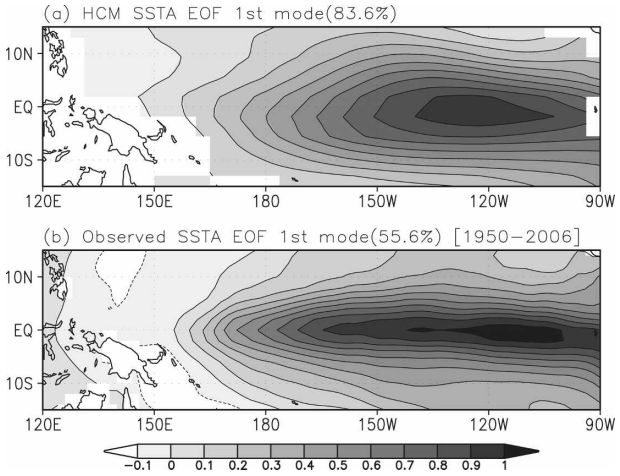

FIG. 2. The first EOF of the SSTA (a) simulated in the HCM for the 159-yr period and (b) for observations during the period from 1950 to 2006.

indicating that the tropics–midlatitude teleconnections are effectively simulated. In addition, Yeh et al. (2004) analyzed intensively the characteristics of interannual and decadal ENSO variability simulated in the HCM. They showed that the spatial structure of the interannual ENSO variability in the HCM is similar to observations. The simulated spectral density for the Niño-3 SST index in the HCM is similar to observation with a peak around 40 months. The El Niño simulated in the HCM has a tendency to be locked to the end of the calendar year. Moreover, fluctuations in the ENSO period and amplitude are significant on decadal time scales, which is evident in observations (Wang and Wang 1996).

We show the leading empirical orthogonal function (EOF) of the SSTA simulated in the HCM for the 159-yr periodfor the assessment of model performance (Fig. 2a). Figure 2b is the same as in Fig. 2a except for the observations during the period from 1950 to 2006. The maximum variance of the model EOF is located in the eastern tropical Pacific, which is slightly shifted to the west compared to the observation. The HCM shows a distinct feature in the meridional scale of the anomaly, which is similar to the observation. The time series of the first EOF principal component (PC) is highly correlated with that of the Niño-3 SST index simulated in the model (not shown). The simulated Niño-3 SST index is reasonable in terms of period, amplitude, and ENSO irregularity compared to observations. One standard deviation of the simulated Niño-3 SST index for the entire simulation period is 0.65°C, which is relatively smaller than the observation (0.79°C). The amplitude of cold and warm events in the model is about −1.5° and 2.5°C, respectively.

4. Results

a. Modes of rainfall variability

To identify the dominant modes of rainfall variability over the East Asia and the WNP region, we first perform an EOF analysis for summer-mean precipitation in observations for the period 1979–2004. Figure 3 shows the first two leading EOFs (i.e., EOF1 and EOF2, Figs. 3a,b) and their corresponding principal components (Figs. 3c,d). For comparison, we include the time series of the Niño-3 SST anomalies and the WNPMI in Figs. 3c,d, respectively.

The EOF1 and EOF2 account for 24.8% and 19.5% of the total summer precipitation variance, respectively. The first two EOFs in observations are clearly separated from the rest according to the criterion of North et al. (1982), indicating that the first two EOFs represent a robust feature of rainfall variability over East Asia. The spatial pattern of the EOF1 is dominated by a large east–west contrast between the Maritime Continent and the equatorial western Pacific. This pattern is similar to that of observed precipitation during the developing phase of ENSO (K05). Indeed, the EOF1 PC time series (solid line in Fig. 3c) is highly correlated to the Niño-3 SST index (dashed line in Fig. 3c) for the period of 1979–2004 with the simultaneous correlation coefficient 0.77. Following K05, we refer to this mode as an ENSO-related mode. On the other hand, the spatial pattern of the EOF2 is characterized by maximum variability over the east of the Philippines. Figure 3b indicates that the anomalous rainfall over the WNP region (10°–20°N, 120°–150°E) is negatively correlated with that over the East Asia region (30°–50°N, 115°–150°E), which is largely consistent with previous studies on the negative simultaneous relationship between the EASM and the WNPSM (Lau et al. 2000; Wang et al. 2001; Lee et al. 2005). The spatial structure of the EOF2 reflects the fluctuations of precipitation and associated latent heat forcing in the WNP monsoon trough (K05). Moreover, the corresponding PC time series (solid line in Fig. 3d) is well correlated with the WNPMI (dotted line in Fig. 3d) with the significantly high correlation coefficient, 0.90. Therefore, we refer to this mode as a WNPSM-related mode. These results indicate that the rainfall variability over the East Asia and WNP region during summer is dominated by two leading modes of variability, that is, an ENSO-related mode (EOF1) and a WNPSM-related mode (EOF2) (Nitta 1986, 1987).

We apply the same analysis to the HCM simulation. Figures 4a–d are the same as Figs. 3a–d except that the data used come from the model simulation. The first

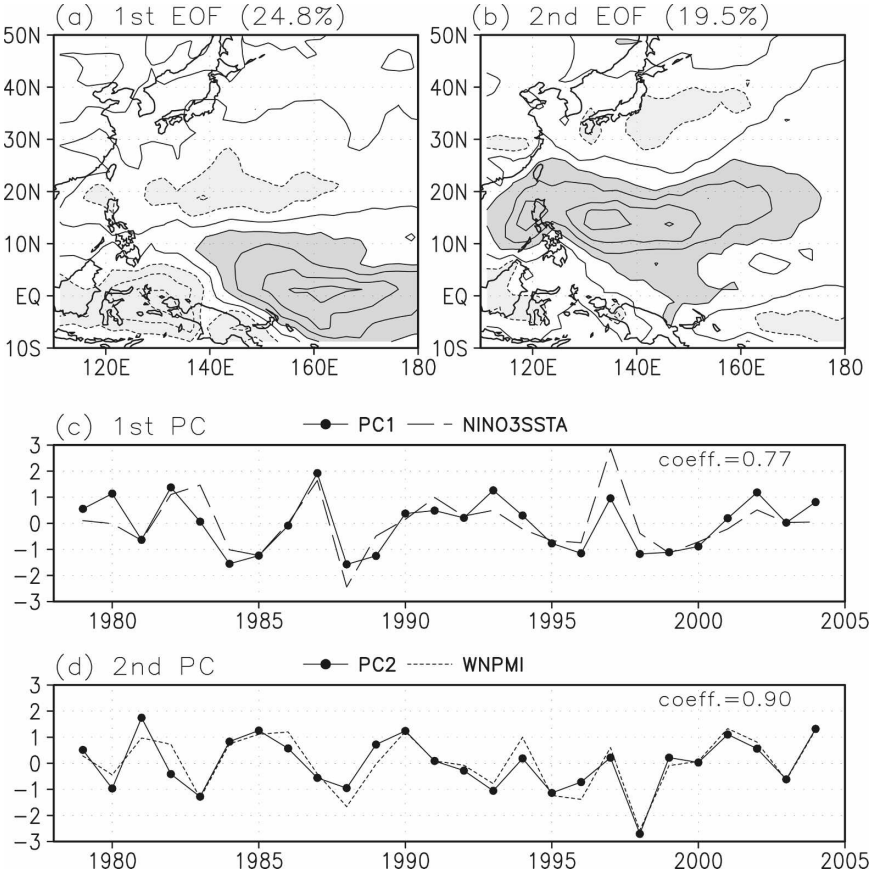

FIG. 3. Eigenvectors of the summer-mean rainfall over a specified region 10°S–50°N, 110°E–180°: (a) the first mode and (b) the second mode for the period 1979–2004. Contour interval is 0.03. (c) The first principal component of the EOF along with JJA-mean Niño-3 SST index. (d) The second principal component of the EOF along with the WNPMI. All principal components, the WNPMI, and the JJA-mean Niño-3 SST index are normalized.

and second leading modes explain 19.7% and 12.3% of total summer precipitation variance, respectively. According to the rule of thumb (North et al. 1982), the first two EOFs in the HCM are well separated from the remaining EOFs. The spatial pattern of EOF1 is characterized by a triplelike structure in the meridional direction. This mode has both similarities to and differences from EOF2 in observations. Both display a large positive loading to the east of the Philippines and a negative loading over East Asia. Differences are seen over the equatorial western Pacific where the model EOF1 has a large negative loading, while the observed EOF2 has a small loading. Interestingly, the EOF1 PC time series (solid line in Fig. 4c) is significantly correlated to the WNPMI simulated in the HCM (dotted line in Fig. 4c) with the simultaneous correlation coefficient, 0.75. This result indicates that the EOF1 mode represents the rainfall variability associated with the WNPSM in the model. On the other hand, the spatial pattern of the EOF2 simulated in the HCM (Fig. 4b) has both similarities to and differences from the EOF1 in observations (Fig. 3a). The simulated EOF2 has a negative loading over the equatorial western Pacific, which is opposite to observations. This discrepancy reflects a systematic bias of the ENSO-related JJA rainfall pattern along the equatorial Pacific in the HCM. In the HCM, ENSO-related JJA rainfall anomalies display an eastward shift of about 30° longitude along the equatorial Pacific, which leads to the appearance of negative rainfall anomalies over the western equatorial Pacific. The simulated EOF2 has a negative loading over the subtropical western North Pacific, which agrees with observations. The magnitude in this region, however, is larger compared to observations. In spite of these discrepancies, the PC time series of the model EOF2 (solid line in Fig. 4d) is well correlated with the

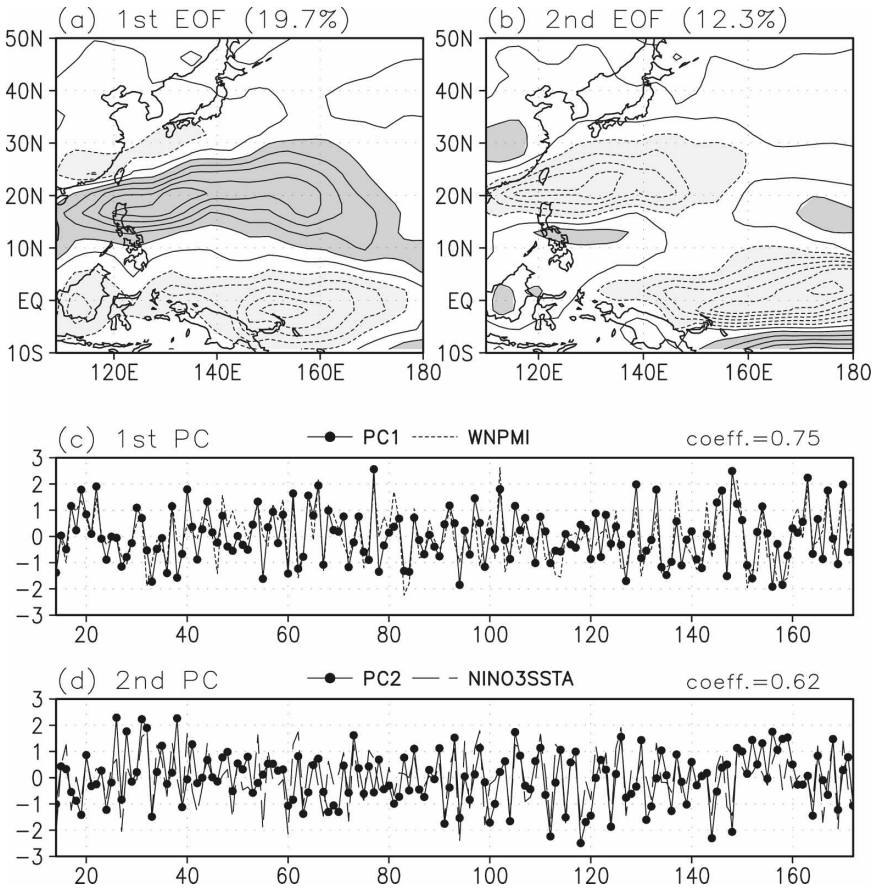

FIG. 4. (a), (b) Same as Figs. 3a,b, but for the summer-mean rainfall anomalies simulated by the HCM for the period of 159 yr. (c) The first principal component of the EOF along with the WNPMI and (d) the second principal component of the EOF along with JJA-mean Niño-3 SST index.

Niño-3 SST index simulated in the HCM (dashed line in Fig. 4d) with a high correlation coefficient, 0.62, significant at the 95% confidence level.

To clarify whether the first two EOFs simulated in the HCM have a physical meaning similar to observations, we project the modeled fields onto the observed EOFs and perform a correlation analysis on the projected time series. Table 1 shows the correlation coefficients between the simulated WNPMI and Niño-3 SST index and the projected time series. The correlation coefficient between the simulated WNPMI and the projected time series onto the observed EOF2 (i.e., a WNPSM-related mode, Fig. 3b) is 0.88 and that between the simulated Niño-3 SST index and the projected time series onto the observed EOF1 (i.e., an ENSO-related mode, Fig. 3a) is −0.65. This negative sign is again due to a systematic bias of the ENSO-related JJA rainfall pattern along the equatorial Pacific in the model compared to the observations. Both correlation coefficients are statistically significant at the 95% confidence level. On the other hand, the correlation coefficients between the simulated WNPMI (Niño-3 SST index) and the projected time series onto the observed EOF1 (EOF2) are not statistically significant. This result suggests that the model can simulate the two different modes, one related to ENSO and the other related to the WNPSM, consistent with observations.

TABLE 1. Correlation coefficients (r) between the simulated indices (i.e., the WNPMI and Niño-3 SST index) and the projected time series.

	Projected time series	
r	Observed EOF1: ENSO-related mode	Observed EOF2: WNPSM-related mode
WNPMI	0.31	0.88
Niño-3 SST index	−0.65	−0.003

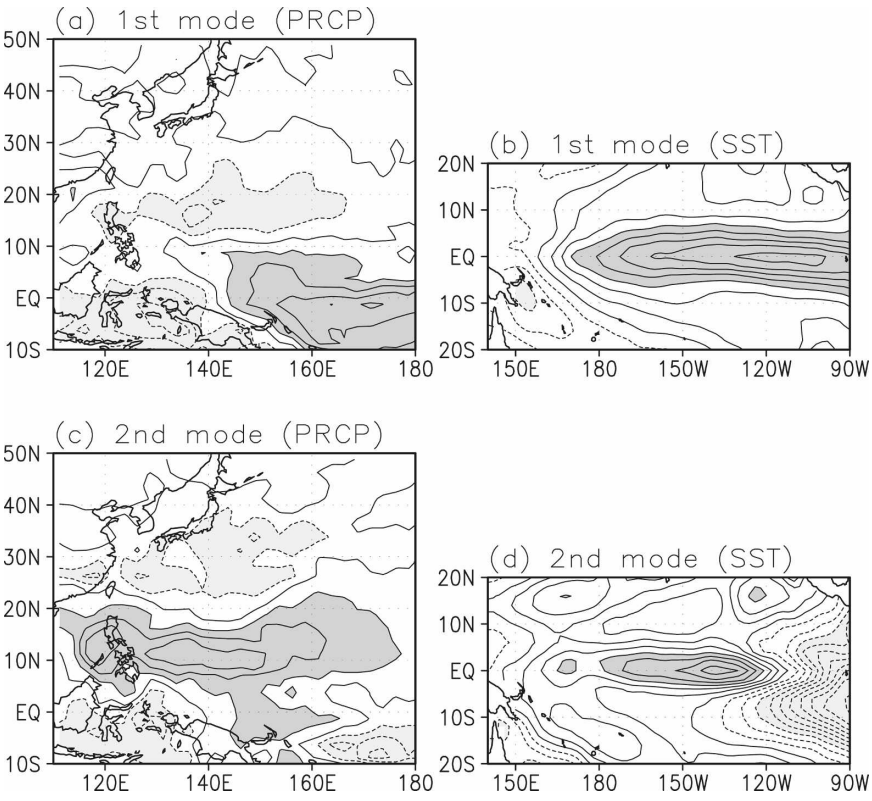

FIG. 5. Horizontal distribution of the (a), (b) first and (c), (d) second CCA modes of summer-mean precipitation and SSTA in observations, respectively. The contour interval for precipitation and SSTA is 0.03 and 0.01, respectively.

For more physical understanding of the first two precipitation EOFs, we perform a canonical correlation analysis (CCA) between the precipitation and the tropical Pacific SSTs for both observations and model simulation. The first CCA mode of precipitation and the tropical Pacific SSTs derived from observations are shown in Figs. 5a,b, and Figs. 5c,d are as in Figs. 5a,b but for the second CCA modes. The first CCA mode of precipitation (Fig. 5a), which quite resembles the ENSO-related mode (i.e., Fig. 3a) in terms of its spatial pattern, is coupled with the El Niño–like SSTA pattern (Fig. 5b). This indicates that the first EOF of precipitation (Fig. 3a) is a mode forced by the tropical Pacific SSTA. On the other hand, the second CCA mode of precipitation (Fig. 5c), which is similar to the WNPSM-related mode (i.e., Fig. 3b), is coupled with a pattern of mixed positive and negative SSTAs in the central and eastern equatorial Pacific. This result suggests that the role of SST forcing for the WNPSM-related mode is much less compared to the ENSO-related mode and the WNPSM-related mode could be more related to internal atmospheric variability. Furthermore, the CCA analysis between the precipitation and the tropical Pacific SSTs based on model simulation (not shown) indicates that the second EOF of precipitation (i.e., the ENSO-related mode, Fig. 4b) is coupled with the ENSO variability in the HCM, whereas the first EOF of precipitation (i.e., the WNPSM-related mode, Fig. 4a) is correlated with a mixed positive and negative SSTA pattern in the equatorial Pacific.

As in observations, the simulated summer rainfall variability in the HCM is dominated by a WNPSM-related mode and an ENSO-related mode. However, different from observations, the WNPSM-related mode (i.e., simulated EOF1) is more dominant than the ENSO-related mode (i.e., simulated EOF2) in the HCM. The reason why the order of the first two EOF modes in the HCM differs from observations might be associated with the difference of ENSO amplitude between the observation and the HCM. We calculated the standard deviation of the Niño-3 SST index during summer in observations (0.59°C) and the HCM (0.41°C). The smaller ENSO amplitude simulated in the HCM than observations may explain why the EOF1 in the observation is related to ENSO, whereas the EOF2 is related to the ENSO in the model. Another plausible factor for the discrepancy in the order of the two leading EOFs in observations and the model is the WNPSM

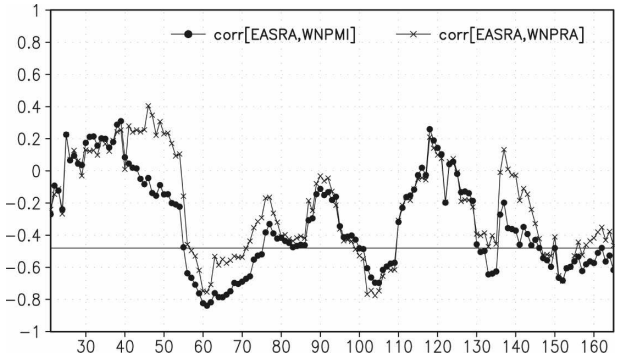

FIG. 6. Sliding correlation coefficients between the East Asian summer rainfall anomaly and WNPMI (thick curve) and between the East Asian summer rainfall anomaly and WNP rainfall anomaly (thin curve) with a window of 15 yr. A horizontal straight line denotes the 95% confidence level.

intensity. For example, a stronger WNPSM in the model may enhance the percent variance explained by the WNPSM-related mode. However, the standard deviation of the WNPMI in observations (i.e., 2.60 m s^{-1}) is slightly larger than that simulated in the HCM (i.e., 2.29 m s^{-1}). This result suggests that the ENSO variability is a key factor in determining the dominant rainfall variability over the East Asia and the WNP region.

b. Changes in the EASM–WNPSM relationship

To show changes in the EASM–WNPSM relationship, a 15-yr sliding correlation coefficient of the time series of the East Asian summer rainfall anomaly and the WNPMI (thick line in Fig. 6) is presented in Fig. 6. Note that the correlation value at the 95% significance level is −0.48, and the mean sliding correlation value for the entire period is −0.32. When the same analysis is applied to the time series of the East Asian summer monsoon rainfall anomaly and the WNP rainfall anomaly (thin line in Fig. 6), similar results are obtained. The most striking feature in Fig. 6 is that the relationship between the EASM and the WNPSM shows apparent decadal variations. There are periods when the EASM–WNPSM is strongly negatively correlated and periods when the EASM–WNPSM is weakly negatively correlated. Moreover, the HCM simulated even a positive relationship between the EASM and the WNPSM during the early simulation period (i.e., model period 25–40 yr).

To further demonstrate changes in the EASM–WNPSM relationship, we compare distinct epochs with a marked difference in the relationship between the EASM and the WNPSM, that is, strongly negatively correlated periods and weakly negatively correlated periods[1] (hereafter period S and period W, respectively). Note that the mean sliding correlation coefficient for period S is −0.64 and for period W, −0.15. We perform EOF analyses for both periods S and W. Table 2 summarizes the explained variances of the WNPSM-related mode and the ENSO-related mode, and its correlation coefficients with the WNPMI and the Niño-3 SST index for the entire period, period S, and period W in the model.

TABLE 2. The explained variances of the WNPSM-related mode and the ENSO-related mode, and the correlation coefficients with the WNPMI and the Niño-3 SST index for the entire period, period S, and period W in the model.

	Explained variance		Correlation coefficient	
	WNPSM-related mode (%)	ENSO-related mode (%)	WNPSM-related mode and WNPMI	ENSO-related mode and Niño-3 SST index
Entire period	19.7	12.3	.75	.62
Period S	26.2	12.1	.85	.66
Period W	15.9	19.5	.69	.87

We first show the dominant modes of summer rainfall variability over the East Asia and the WNP region during period S and period W. Figures 7a–d are as in Figs. 4a–d, but for period S. The first and second leading EOFs for period S (Figs. 7a,b) account for 26.2% and 12.1% of total variance, respectively. The spatial pattern of the EOF1 and EOF2 for period S shares very similar structure with the WNPSM-related mode (Fig. 4a) and the ENSO-related mode (Fig. 4b) for the entire period, respectively. The EOF1 (Fig. 7a) is characterized by a triplelike structure in the meridional direction, and the EOF2 (Fig. 7b) is dominated by the maximum variance of rainfall anomalies in the equatorial western Pacific, which is largely consistent with Figs. 4a,b. The simultaneous correlation coefficient between the EOF1 PC time series and the WNPMI for period S is 0.85 (Fig. 7c) and that between the EOF2 PC time series and the Niño-3 SST index for period S is 0.66 (Fig. 7d), both statistically significant at the 95% confidence level. It is noteworthy that the explained vari-

[1] Strong correlated periods of the EASM–WNPSM are based on periods when the sliding correlation coefficients between the East Asian summer rainfall anomaly and WNPMI exceed −0.48 (i.e., 95% significance confidence level). The model years 56–75 and 147–165 are chosen as the strong periods. On the other hand, weak correlated periods of the EASM–WNPSM are based on periods when the sliding correlation coefficients do not exceed −0.48 with somewhat long-lasting periods. The model years 88–97 and 110–130 are chosen as the weak periods.

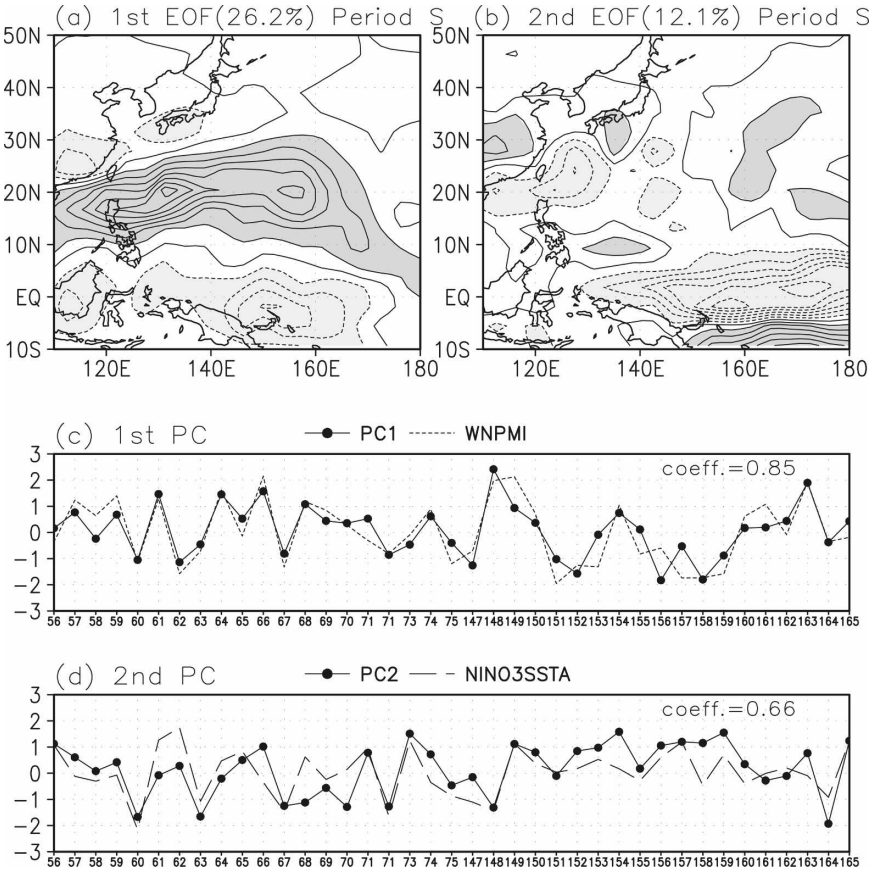

FIG. 7. Same as Fig. 4, but for the period S.

ance of the WNPSM-related mode for period S increases from 19.7% to 26.2%, and the simultaneous correlation coefficient with the WNPMI also increases from 0.75 to 0.85 compared to the entire period (Table 2). On the other hand, the explained variance of the ENSO-related mode (EOF2) and the correlation coefficient of the EOF2 PC with the Niño-3 SST index are not much different between period S and the entire period. These results indicate that the rainfall variability associated with the WNPSM increases over the East Asia and WNP region for period S compared to the entire period.

For period W, the most dominant mode of summer rainfall variability over the East Asia and WNP region is associated with ENSO. Figures 8a–d are as in Figs. 5a–d but for period W. For period W the EOF1 (Fig. 8a) and EOF2 (Fig. 8b) represent the rainfall variability associated with ENSO and the WNPSM, respectively, which is a reversed relationship compared to the entire period and period S. The pattern correlation between the EOF1 in period W (Fig. 8a) and the EOF2 in the entire period (i.e., the ENSO-related mode; Fig. 4b) is 0.87. The simultaneous correlation coefficient between the EOF1 PC time series and the Niño-3 SST index is 0.87 (Fig. 8c) and that between the EOF2 PC time series and the WNPMI is 0.69 (Fig. 8d).[2] Both the explained variance of the ENSO-related mode (19.5%) and the simultaneous correlation coefficient between its PC time series and the Niño-3 SST index (0.87) for period W increase compared to the entire period (i.e., 12.3% and 0.62; Table 2). On the other hand, the explained variance of the WNPSM-related mode (15.9%) and the simultaneous correlation coefficient with the WNPMI (0.69) for period W decreases compared to the entire period (i.e., 19.7% and 0.75; Table 2).

A similar result has been obtained by K05 in observations. K05 showed that the explained variance of the WNPSM-related mode is 38.26% and that of the ENSO-related mode is 16.68% for period S (i.e., 1994–

[2] The correlation coefficient between the EOF1 PC time series and the WNPMI is 0.27 and between the EOF2 PC time series and the Niño-3 SST index, 0.02.

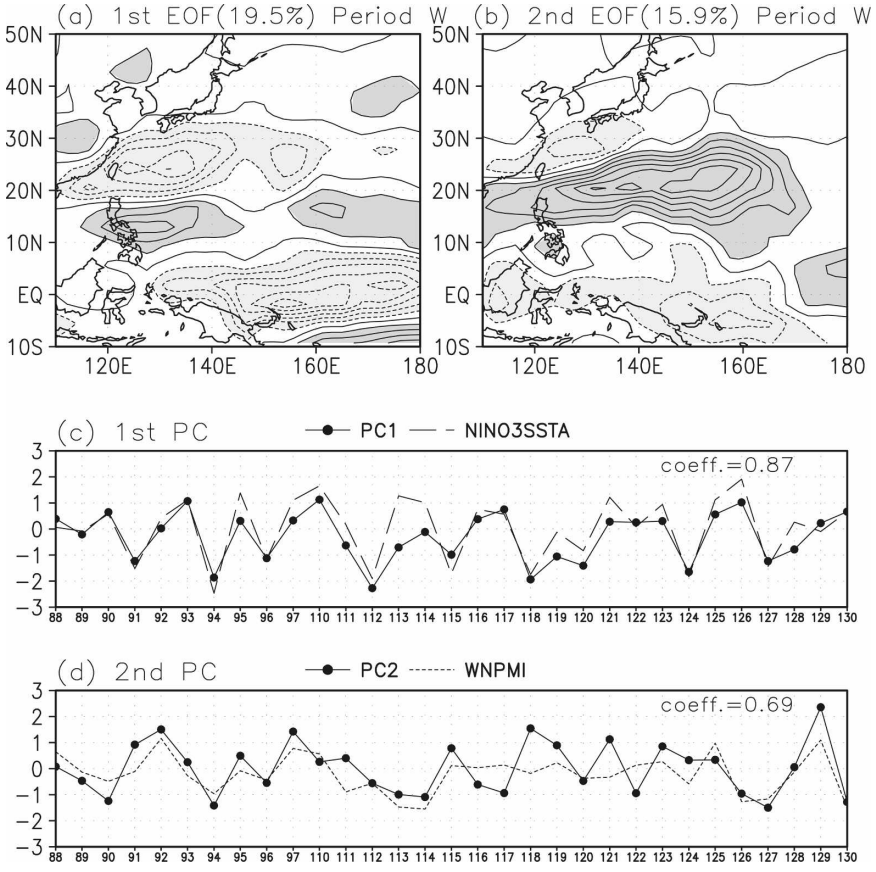

FIG. 8. Same as Fig. 4, but for the period W.

2004). For period W (i.e., 1979–93), in contrast, the explained variance of the WNPSM-related mode is 13.86% and that of the ENSO-related mode is 36.7%. Again, the rainfall variability associated with the WNPSM increases over the East Asia and WNP region for period S and vice versa for period W in observations.

Gershunov et al. (2001) suggested that stochastic processes can induce large changes in the sliding correlation. To check this possibility, we examine the changes in the sliding EASM–WNPSM correlation based on the Gershunov et al. (2001) test. The standard deviation of the correlation time series shown in Fig. 6 is 0.30, slightly below the 95% confidence level in a one-tailed test according to Gershunov et al.[3] Therefore, we infer that stochastic processes may also have contributions to variations in the EASM–WNPSM correlation.

c. *Plausible mechanism for changes in the EASM–WNPSM relationship*

Previous studies have suggested that the EASM tends to be correlated negatively with the WNPSM (Lau et al. 2000; Wang et al. 2001; Wu and Wang 2002; Wu et al. 2003; Lee et al. 2005). K05 identified a decadal change in the relationship between the EASM and the WNPSM around 1993–94. Based on a much longer time series from a HCM, we suggest that there is a robust low-frequency modulation in the relationship between the EASM and the WNPSM. Understanding such changes in the relationship between the EASM and the WNPSM may be very useful for better prediction of the interannual variability of the Asian–Pacific summer monsoon system. In this subsection we investigate potential physical mechanisms for decadal variations in the relationship between the EASM and the WNPSM.

The results in the previous subsection clearly indicate that the summer-mean precipitation variability over the East Asia and the WNP region is more attributed to the WNPSM for period S and more to the ENSO for period W. In other words, the more the precipitation variabil-

[3] Note that the 95 and 5 percentile confidence limits of the time series shown in Fig. 6 are 0.31 and 0.16, respectively. The std devs must be outside these limits to be considered significant.

TABLE 3. Std dev of the WNP rainfall anomaly time series and the Niño-3 SST index for period S and period W in observations and in the model.

	Observation		Model	
	WNP rainfall anomaly (mm day^{-1})	Niño-3 SST index (°C)	WNP rainfall anomaly (mm day^{-1})	Niño-3 SST index (°C)
Period S	1.99	0.81	1.81	0.58
Period W	1.88	0.81	1.37	0.77

ity associated with the WNPSM (ENSO) is enhanced over the East Asia and WNP region, the stronger (weaker) is the relationship between the EASM and the WNPSM. This implies the possibility that changes in the EASM–WNPSM relationship may be related to changes in the variability of the WNPSM and ENSO. For example, a stronger WNPSM may impose a larger impact on the EASM, which in turn may lead to a stronger EASM–WNPSM correlation.

To support this argument, we count the number of extreme rainfall events associated with the WNPSM for period S and period W. The extreme rainfall events are based on the time series of the WNP rainfall anomaly either exceeding one standard deviation or being less than minus one standard deviation. Note that the WNP rainfall anomaly is defined by the summer-mean rainfall anomaly averaged over the WNP region (10°–20°N, 120°–150°E). The number of extreme rainfall events for period S (i.e., 20) is more than two times as many as that for period W (i.e., 8), suggesting that the precipitation variability associated with the WNPSM is quite large for period S compared to period W. Furthermore, we calculated the standard deviation of the time series of the WNP rainfall anomaly for period S and period W. The rainfall amplitude over the WNP region for period S is 1.81 mm day^{-1}, which is much larger than that for period W [1.37 mm day^{-1} (Table 3)], suggesting that the rainfall variability associated with the WNPSM is reduced over the East Asia and WNP region from period S to period W. This is consistent with the result that the explained variance of the WNPSM-related mode for period S is higher than that for period W. Similar relationships can be found in observations. Based on the results in K05, we compared the standard deviation of the time series of the WNP rainfall anomaly in observations for the period 1994–2004 (i.e., strong period) and for the period 1979–93 (i.e., weak period). The rainfall amplitude associated with the WNPSM for the period 1994–2004 is 1.99 mm day^{-1}, which is larger than that for the period 1979–93 [1.88 mm day^{-1} (Table 3)].

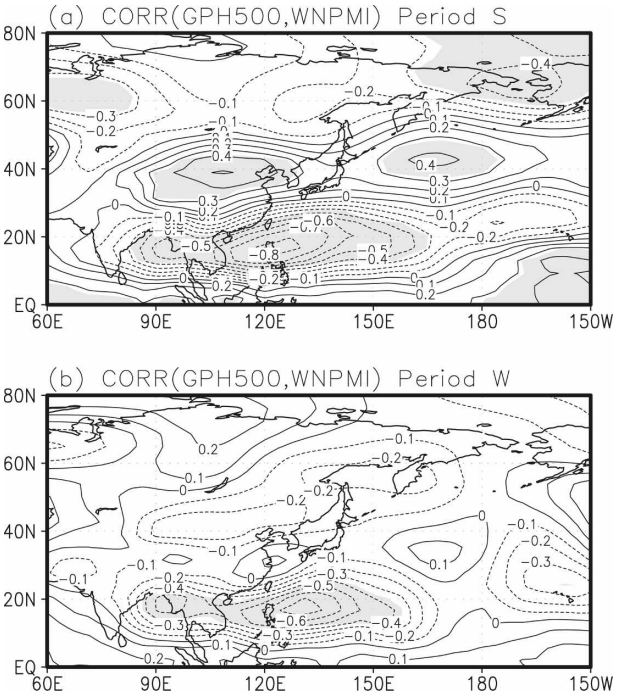

FIG. 9. Maps of correlation coefficients between the JJA-mean geopotential height at 500 hPa and the WNPMI (a) for the period S and (b) for the period W. The regions exceeding the 95% confidence level are shaded.

Large variability in precipitation associated with the WNPSM is connected with the strength of atmospheric teleconnections between the East Asia region and the WNP region. Wang et al. (2001) suggested that convective activities over the WNP region are associated with the stationary wavelike pattern in the midlatitudes. Figures 9a and 9b show maps of the simultaneous correlation between the summer-mean geopotential height at 500 hPa and the WNPMI for period S and period W. Note that the shading indicates the statistically significant regions exceeding the 95% confidence level. The most striking features between the two periods are in the Pacific–Japan (PJ)-like pattern (Nitta 1987) of the 500-hPa geopotential height in the meridional direction. For period S the two polarities of the PJ-like pattern are located in the Philippine Sea and the northeast Asian region. The anomalous high over northeastern China, Korea, and Japan emerges in a strong WNPSM. The pattern bears a resemblance to a barotropic Rossby wave response to a subtropical forcing near the Philippines (Huang and Sun 1992). For period W, however, the significant geopotential height at 500 hPa associated with the WNPMI is zonally localized within the WNP region and the Bay of Bengal. There is no significant atmospheric teleconnections between the WNP region and the East Asia region, although overall spatial struc-

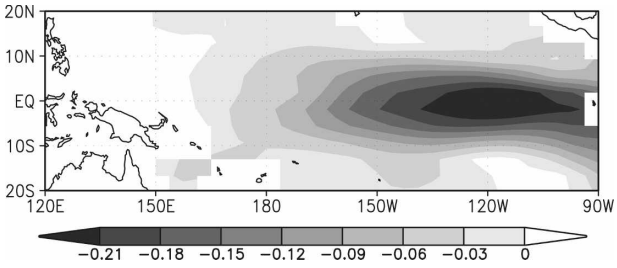

FIG. 10. Difference in the SSTA std dev between period S and period W.

ture of the 500-hPa geopotential height is reminiscent with the PJ-like pattern. Compared to period S, the anomalous high over the East Asia region is weak and even negative anomalies appear over northeastern China and Korea. This explains the weak negative relationship between the EASM and the WNPSM. The processes of how the WNPSM influences the EASM could be as follows: the WNP convective heating generates a meridional teleconnection pattern, as suggested in previous studies (i.e., the PJ-like pattern; Nitta 1986, 1987), and this induces height anomalies over East Asia. Such atmospheric circulation anomalies then affect the rainfall anomalies over East Asia.

We argue that the summer-mean precipitation variability over the East Asia and the WNP region is more associated with ENSO than with the WNPSM for period W. Here we show the difference in the SSTA standard deviation between period S and period W (Fig. 10). The SSTA standard deviation is largely reduced in the equatorial Pacific basin for period S compared to period W and the maximum differences are located in the eastern tropical Pacific. The spatial structure of differences of SSTA standard deviation between the two periods is similar to that of the first EOF of the SSTA simulated in the HCM (Fig. 2a), indicating that ENSO variability for period S is weak and vice versa for period W. As expected, the standard deviation of the Niño-3 SST index for period S is 0.58°C, which is smaller than that for period W (0.77°C, Table 3). Large ENSO variability for period W may contribute to the increase in precipitation variability associated with ENSO over the East Asia and WNP regions. As a result, the most dominant mode of rainfall variability over the East Asia and the WNP region becomes the ENSO-related mode for period W. We also calculated the 15-yr window Niño-3 SST index variance over the same period (thin line in Fig. 11) and compared it with the time series of the 15-yr sliding correlation between the East Asian summer rainfall anomaly and the WNPMI (thick line in Fig. 11). From Fig. 11, it is clear that the two weakest correlation periods correspond to periods of large ENSO variability. The strong correlation periods, however,

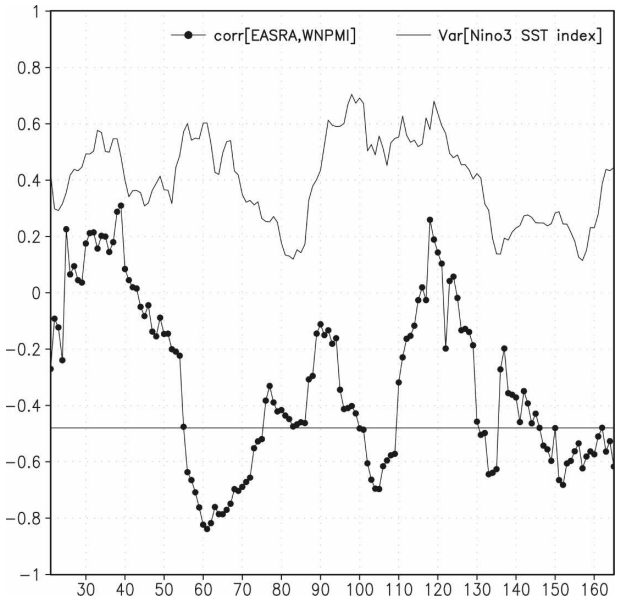

FIG. 11. Time series of the 15-yr window Niño-3 SST index variance (thin) and the 15-yr sliding correlation coefficient of the East Asian summer rainfall anomaly and the WNPMI (thick).

are not necessarily associated with weak ENSO variability, suggesting that ENSO is not the only factor for changes in the EASM–WNPSM relationship. We speculate that the rainfall variability due to enhanced ENSO variability may interfere with the WNPSM-related rainfall variability over the East Asia and the WNP region, resulting in a weakened relationship between the EASM and the WNPSM in the meridional direction. We applied the same calculation to observations and compared the standard deviation of the Niño-3 SST index in observations for the periods 1994–2004 and 1979–93. Unlike the model, the standard deviation of the Niño-3 SST index for the period 1994–2004 (0.81°C) is similar to that for 1979–93 (0.81°C, Table 3). In spite of little difference in the Niño-3 SST variance between the two epochs, according to K05, the explained variance of the ENSO-related mode for the period 1994–2004 (i.e., strong period) is smaller than that for 1979–93 (i.e., weak period).

In summary, the change in the WNPSM–EASM relationship could be related to changes in the magnitude of both the Niño-3 SST index and WNP rainfall anomaly. In the model, both effects favor our argument. In observations, the ENSO effect is not favorable for this relationship change, but the WNPRA effect is favorable, although changes in the WNP rainfall anomaly amplitude are not as large as in the model. In other words, a larger WNP rainfall anomaly variability could lead to a stronger WNPSM–EASM relationship, although the ENSO effect is the same.

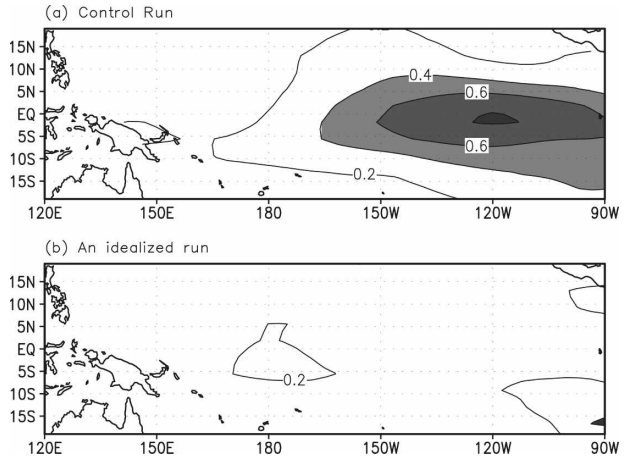

FIG. 12. Std dev of the JJA SSTA simulated in (a) the control run and (b) the idealized run for the entire analyzed period. Contour interval is 0.2°C; shading is above 0.4°C.

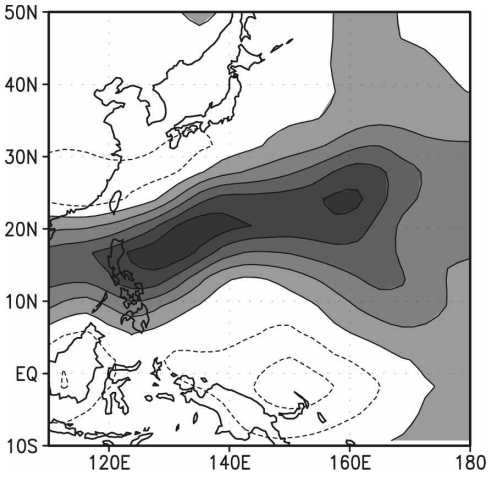

FIG. 13. The first leading mode for summer-mean precipitation in the idealized run and its explained variance (27.2%). Shading is for positive loading; contour interval is 0.03.

d. An idealized model experiment

In the previous section, we hypothesized that the rainfall variability due to enhanced ENSO variability can destructively interfere with the relationship between the EASM and the WNPSM. A stronger ENSO may impose a larger impact on rainfall variability over the East Asia and WNP region, which in turn may lead to a weaker EASM–WNPSM correlation. To test this hypothesis we conduct an idealized run in which the ENSO is shut down in the model. In this run, the thermocline depth anomaly is set to zero in the model, following the methodology of Xie and Saito (2001). We run the model for a period of 50 years.

Figures 12a and 12b show the standard deviation of the JJA SSTA simulated in the control run and the idealized run for the entire analyzed period. As expected, the SSTA variability is greatly reduced in the idealized run compared to the control run, indicating that the ENSO is mostly suppressed in the idealized run. The standard deviation of simulated JJA Niño-3 SST index in the control run is 0.67°C and in the idealized run 0.13°C. Figure 13 shows the first leading mode for summer-mean precipitation in the idealized run and it explains 27.2% of the total summer precipitation variance. The spatial pattern of the EOF1 (Fig. 13) is quite similar to that of the WNPSM-related mode (Fig. 4a) simulated in the control run for the entire analyzed period. The EOF1 is characterized by a triple-like structure in the meridional direction and displays a large positive loading to the east of the Philippines and two negative loadings over the equatorial western Pacific and East Asia. The pattern correlation between the EOF1 (Fig. 13) and the WNPSM-related mode simulated in the control run (Fig. 4a) is high, 0.87. Furthermore, the EOF1 PC time series are significantly correlated with the simulated WNPMI with a simultaneous correlation coefficient, 0.93, suggesting that the EOF1 represents a WNPSM-related mode in the idealized run. The explained variance of the WNPSM-related mode increases from 19.7% in the control run to 27.2% in the idealized run, suggesting that a stronger WNPSM enhances the percent variance explained by the WNPSM-related mode in the idealized run. Furthermore, the correlation coefficient of the time series of the East Asian summer rainfall anomaly and the WNPMI for the entire analyzed period is −0.57 in the idealized run, significant at the 95% confidence level. This correlation coefficient is higher than that in the control run for the entire analyzed period (−0.33). The results of this experiment support our hypothesis that a stronger WNPSM–EASM relationship could be possible when the ENSO is suppressed.

5. Summary

Understanding the relationship between the submonsoon systems and its decadal changes is important to predict the interannual variability of the Asian–Pacific summer monsoon. Recently, K05 found that the negative relationship between the EASM and the WNPSM is much stronger in the recent decade (1994–2004) than in the epoch before 1994 (1979–93). Owing to limited data availability,[4] however, it is unclear how significant is the low frequency modulation in the relationship between the EASM and the WNPSM. Using a much

[4] We also extended the analysis of the observed EASM–WNPSM relationship using longer records. The EASM index is constructed based on land-only precipitation from the Climate

longer time series from the HCM, we investigated decadal variations in the relationship between the two submonsoon systems.

There are two distinct modes of rainfall variability simulated in the HCM over the East Asia and the WNP region, that is, a WNPSM-related mode and an ENSO-related mode, which are consistent with observations except for the relative explained variance. The WNPSM-related mode of variability is highly correlated with the WNPMI. On the other hand, the ENSO-related mode of variability has a significant simultaneous correlation with the simulated Niño-3 SST index in the HCM. Unlike observations, the rainfall variability associated with the WNPSM is more dominant than the ENSO-related variability for the entire period in the HCM. Based on the sliding correlation coefficients of the East Asian summer rainfall anomaly and the WNPMI, it is found that decadal variations are apparent in the relationship between the EASM and the WNPSM in the HCM. On decadal time scales there are periods when the EASM–WNPSM is strongly negatively correlated (i.e., period S) and periods when the EASM–WNPSM is weakly negatively correlated (i.e., period W). For period S the WNPSM-related mode of rainfall variability is enhanced over the East Asia and the WNP region. In contrast, for period W the ENSO-related mode of rainfall variability is enhanced compared to the entire period. The dominant mode of rainfall variability is associated with the WNPSM (ENSO) over the East Asia and the WNP region for period S (W). This result indicates that the precipitation variability associated with the WNPSM (ENSO) is enhanced over the East Asia and WNP regions when the relationship between the EASM and the WNPSM is stronger (weaker).

Large variability in precipitation associated with the WNPSM is connected with the strength of atmospheric teleconnections between the East Asia and the WNP regions. The PJ-like pattern of the 500-hPa geopotential height is significant for period S, but it is localized within the WNP region and the atmospheric linkage over the East Asia region is weak for period W. We argue that the relationship between the EASM and the WNPSM for period S is largely dependent on an enhancement or reduction of the precipitation variability associated with the WNPSM over the East Asia and the WNP region. On the other hand, the summer-mean precipitation variability over the East Asia and WNP region is more closely linked with ENSO than with the WNPSM for period W. The ENSO amplitude is largely enhanced in period W compared to period S, which increases the precipitation variability associated with ENSO over the East Asia and the WNP region. We speculate that the rainfall variability due to enhanced ENSO variability interferes with the WNPSM-related rainfall variability over the East Asia and the WNP region, resulting in a weakening in the relationship between the EASM and the WNPSM. To support this speculation we conducted an idealized experiment where the ENSO is suppressed by switching off the thermocline–SST feedback in the model. A stronger WNPSM enhances the percent variance explained by the WNPSM-related mode in the idealized run. Furthermore, the EASM–WNPSM relationship is stronger in the idealized run than that in the control run, suggesting that a larger WNP rainfall anomaly variability leads to a stronger WNPSM–EASM relationship when the ENSO is suppressed.

Acknowledgments. This work was funded by the Korea Meteorological Administration Research and Development Program under Grant CATER 2006-4205. The research was also supported by Brain Korea 21 Project in School of Earth and Environmental Sciences of Seoul National University. The authors appreciate insightful comments by two anonymous reviewers that led to a significant improvement of this manuscript.

REFERENCES

Chang, C.-P., Y. Zhang, and T. Li, 2000: Interannual and interdecadal variations of the East Asian summer monsoon and tropical Pacific SSTs. Part I: Roles of the subtropical ridge. *J. Climate,* **13,** 4310–4325.

Chen, L.-X., M. Dong, and Y.-N. Shao, 1992: The characteristics of interannual variations on the East Asian monsoon. *J. Meteor. Soc. Japan,* **70,** 397–421.

Gershunov, A., N. Schneider, and T. P. Barnett, 2001: Low-frequency modulation of the ENSO–Indian monsoon rainfall relationship: Signal and noise? *J. Climate,* **14,** 2486–2492.

Graham, N. E., 1994: Decadal-scale climate variability in the tropical and North Pacific during the 1970s and 1980s: Observations and model results. *Climate Dyn.,* **10,** 135–162.

Huang, B., and J. Shukla, 1997: Characteristics of the interannual and decadal variability in a general circulation model of the tropical Atlantic Ocean. *J. Phys. Oceanogr.,* **27,** 1693–1712.

Huang, R. H., and Y.-F. Wu, 1989: The influence of ENSO on the summer climate change in China and its mechanism. *Adv. Atmos. Sci.,* **6,** 21–32.

——, and F. Sun, 1992: Impacts of the tropical western Pacific on

Research Unit data (New et al. 2000) for the period of 1948–2002. The dynamical index for the WNPSM is constructed from the NCEP reanalysis. The decadal variations in the EASM–WNPSM relationship are readily apparent, although sliding correlation coefficients are weaker compared to the model (not shown). However, it is still difficult to apply our hypothesis to these results because distinct epochs with a marked difference in the EASM–WNPSM relationship are relatively short and not suitable for a comparison and the precipitation variance is much larger over the ocean than over land.

the East Asian summer monsoon. *J. Meteor. Soc. Japan,* **70,** 243–256.

Kalnay, E., and Coauthors, 1996: The NCEP/NCAR 40-Year Reanalysis Project. *Bull. Amer. Meteor. Soc.,* **77,** 437–471.

Kang, I.-S., and Coauthors, 2002: Intercomparison of atmospheric GCM simulated anomalies associated with the 1997/98 El Niño. *J. Climate,* **15,** 2791–2805.

Kim, J.-K., I.-S. Kang, and C.-H. Ho, 1998: East Asian summer monsoon simulated by the Seoul National University GCM. *Proc. Int. Conf. on Monsoon and Hydrologic Cycle,* Kyongju, South Korea, Korean Meteorological Society, 227–231.

Kirtman, B. P., and S. Zebiak, 1997: ENSO simulation and prediction with a hybrid coupled model. *Mon. Wea. Rev.,* **125,** 2620–2641.

Kripalani, R. H., and A. Kulkarni, 2001: Monsoon rainfall variations and teleconnections over South and East Asia. *Int. J. Climatol.,* **21,** 603–616.

Krishnamurti, T. N., 1985: Summer monsoon experiment—A review. *Mon. Wea. Rev.,* **113,** 1590–1626.

Krishnan, R., and M. Sugi, 2001: Baiu rainfall variability and associated monsoon teleconnection. *J. Meteor. Soc. Japan,* **79,** 851–860.

Kwon, M., J.-G. Jhun, B. Wang, S.-I. An, and J.-S. Kug, 2005: Decadal change in relationship between east Asian and WNP summer monsoons. *Geophys. Res. Lett.,* **32,** L16709, doi:10.1029/2005GL023026.

Lau, K.-M., and H. Weng, 2001: Coherent modes of global SST and summer rainfall over China: An assessment of the regional impacts of the 1997–98 El Niño. *J. Climate,* **14,** 1294–1308.

——, K.-M. Kim, and S. Yang, 2000: Dynamical and boundary forcing characteristics of regional components of the Asian summer monsoon. *J. Climate,* **13,** 2461–2482.

Lee, E.-J., J.-G. Jhun, and C.-K. Park, 2005: Remote connection of the northeast Asian summer rainfall variation revealed by a newly defined monsoon index. *J. Climate,* **18,** 4381–4393.

——, S.-W. Yeh, J.-G. Jhun, and B.-K. Moon, 2006: Seasonal change in anomalous WNPSH associated with the strong East Asian summer monsoon. *Geophys. Res. Lett.,* **33,** L21702, doi:10.1029/2006GL027474.

Liu, Y., and Y. H. Ding, 1992: Influence of El Niño on weather and climate in China. *Acta Meteor. Sin.,* **6,** 117–131.

Lu, R., 2004: Associations among the components of the East Asian summer monsoon system in the meridional direction. *J. Meteor. Soc. Japan,* **82,** 155–165.

Murakami, T., and J. Matsumoto, 1994: Summer monsoon over the Asian continent and the western North Pacific. *J. Meteor. Soc. Japan,* **72,** 719–745.

New, M., M. Hulme, and P. D. Jones, 2000: Representing twentieth-century space–time climate variability. Part II: Development of 1901–96 monthly grids of terrestrial surface climate. *J. Climate,* **12,** 2217–2238.

Nitta, T., 1986: Long term variations of cloud amount in the western Pacific region. *J. Meteor. Soc. Japan,* **64,** 373–390.

——, 1987: Convective activities in the tropical western Pacific and their impact on the Northern Hemisphere summer circulation. *J. Meteor. Soc. Japan,* **65,** 373–390.

North, G. R., T. L. Bell, R. F. Cahalan, and F. J. Moeng, 1982: Sampling errors in the estimation of empirical orthogonal functions. *Mon. Wea. Rev.,* **110,** 699–706.

Numaguti, A., M. Takahashi, T. Nakajima, and A. Sumi, 1995: Development of an atmospheric general circulation model. *Climate System Dynamics and Modelling,* Vols. 1–3, T. Matsuno, Ed., University of Tokyo, 1–27.

Shen, S.-H., and K.-M. Lau, 1995: Biennial oscillation associated with the East Asian summer monsoon and tropical sea surface temperature. *J. Meteor. Soc. Japan,* **73,** 105–124.

Smith, T. M., and R. W. Reynolds, 2004: Improved extended reconstruction of SST (1854–1997). *J. Climate,* **17,** 2466–2477.

Tao, S., and L. Chen, 1987: A review of recent research on the East Asia summer monsoon in China. *Monsoon Meteorology,* C.-P. Chang and T. N. Krishnamurti, Eds., Clarendon Press, 60–92.

Terray, P., P. Delecluse, S. Labattu, and L. Terray, 2003: Sea surface temperature associations with the late Indian summer monsoon. *Climate Dyn.,* **21,** 593–618.

Wang, B., and Y. Wang, 1996: Temporal structure of the Southern Oscillation as revealed by waveform and wavelet analysis. *J. Climate,* **9,** 1586–1598.

——, and X. Xu, 1997: Northern Hemisphere summer monsoon singularities and climatological intraseasonal oscillation. *J. Climate,* **10,** 1071–1085.

——, and Z. Fan, 1999: Choice of south Asian summer monsoon indices. *Bull. Amer. Meteor. Soc.,* **80,** 629–638.

——, and LinHo, 2002: Rainy season of the Asian–Pacific summer monsoon. *J. Climate,* **15,** 386–398.

——, R. Wu, and X. Fu, 2000: Pacific–East Asian teleconnection: How does ENSO affect East Asian climate? *J. Climate,* **13,** 1517–1536.

——, ——, and K.-M. Lau, 2001: Interannual variability of the Asian summer monsoon: Contrasts between the Indian and the western North Pacific–East Asian monsoons. *J. Climate,* **14,** 4073–4090.

——, ——, and T. Li, 2003: Atmosphere–warm ocean interaction and its impacts on the Asian–Australian monsoon variation. *J. Climate,* **16,** 1195–1211.

Wu, R., and B. Wang, 2000: Interannual variability of summer monsoon onset over the western North Pacific and the underlying processes. *J. Climate,* **13,** 2483–2501.

——, and ——, 2002: A contrast of the East Asian summer monsoon–ENSO relationship between 1962–77 and 1978–93. *J. Climate,* **15,** 3266–3279.

——, Z.-Z. Hu, and B. P. Kirtman, 2003: Evolution of ENSO-related rainfall anomalies in East Asia. *J. Climate,* **16,** 3742–3758.

Xie, P., and P. A. Arkin, 1997: Global precipitation: A 17-year monthly analysis based on gauge observations, satellite estimates, and numerical model outputs. *Bull. Amer. Meteor. Soc.,* **78,** 2539–2558.

Xie, S.-P., and K. Saito, 2001: Formation and variability of a northerly ITCZ in a hybrid coupled AGCM: Continental forcing and oceanic–atmospheric feedback. *J. Climate,* **14,** 1262–1276.

Yeh, S.-W., 2001: Dynamical impacts of atmospheric and oceanic modes on the ENSO variability: Modeling and theory. Ph.D. dissertation, Seoul National University, 152 pp.

——, J.-G. Jhun, I.-S. Kang, and B. P. Kirtman, 2004: The decadal ENSO variability in a hybrid coupled model. *J. Climate,* **17,** 1225–1238.

Yoo, S.-H., C.-H. Ho, S. Yang, H.-J. Choi, and J.-G. Jhun, 2004: Influences of tropical western and extratropical Pacific SST on east and southeast Asian climate in the summers of 1993–94. *J. Climate,* **17,** 2673–2687.

Zebiak, S. E., and M. A. Cane, 1987: A model El Niño–Southern Oscillation. *Mon. Wea. Rev.,* **115,** 2262–2278.

Zhang, R., A. Sumi, and M. Kimoto, 1996: Impact of El Niño on the East Asian monsoon: A diagnostic study of the '86/87 and '91/92 events. *J. Meteor. Soc. Japan,* **74,** 49–62.